

# Rapid evolution and biogeographic spread in a colorectal cancer

Joao M Alves<sup>1,2,3</sup>, Sonia Prado-Lopez<sup>1,2,3</sup>, Jose Manuel Cameselle-Teijeiro<sup>4,5</sup>, David Posada<sup>\*,1,2,3</sup>

1. Department of Biochemistry, Genetics and Immunology, University of Vigo, Spain.
2. Biomedical Research Center (CINBIO), University of Vigo, Spain.
3. Galicia Sur Health Research Institute, Vigo, Spain.
4. Department of Pathology, Clinical University Hospital, Galician Healthcare Service (SERGAS), Santiago de Compostela, Spain.
5. Medical Faculty, University of Santiago de Compostela, Santiago de Compostela, Spain

\* Corresponding author: [dposada@uvigo.es](mailto:dposada@uvigo.es)

**Keywords:** tumor phylogenetics, cancer evolution, biogeography, colorectal cancer, metastatic dissemination

## ABSTRACT

1 **How and when tumoral clones start spreading to surrounding and distant tissues is currently**  
2 **unclear. Here, we leveraged a model-based evolutionary framework to investigate the**  
3 **demographic and biogeographic history of a colorectal cancer. Our analyses strongly support**  
4 **an early monoclonal metastatic colonization, followed by a rapid population expansion at both**  
5 **primary and secondary sites. Moreover, we infer a hematogenous metastatic spread seemingly**  
6 **under positive selection, plus the return of some tumoral cells from the liver back to the colon**  
7 **lymph nodes. This study illustrates how sophisticated techniques typical of organismal**  
8 **evolution can provide a detailed picture of the complex tumoral dynamics over time and space.**

9 Cancer has long been recognized as a somatic evolutionary process mainly driven by continuous  
10 Darwinian natural selection, in which cells compete for space and resources<sup>1</sup>. With the increasing  
11 availability of high-throughput genomic data, several studies have started to explore the  
12 evolutionary relationships of tumor clones in order to identify the key molecular changes driving  
13 cancer progression<sup>2</sup>, to better understand the subclonal architecture of tumors<sup>3,4</sup>, and to  
14 determine the origins of metastases<sup>5</sup>. While sophisticated inferential methods have been put  
15 forward that make use of sequencing data to investigate the timing and the patterns of  
16 geographical dispersal of organismal lineages<sup>6,7</sup>, their application in cancer research has only  
17 recently started<sup>8,9</sup>.

18  
19 In metastatic colorectal cancer (mCRC) many aspects underlying the dissemination of cancer cells  
20 to tissues beyond primary lesions have been difficult to determine. Although earlier models of  
21 mCRC progression have proposed a sequential metastatic cascade, with cells from the primary

22 tumor first escaping to local lymph nodes from where they seed distant tissues<sup>10</sup>, conflicting  
23 evidence has recently emerged, as some genomic datasets seem to favor an independent origin  
24 of distant and lymph node metastases<sup>5</sup>. Here, to better understand the tempo and mode of  
25 diversification of the tumoral cells within the human body, we sampled and analyzed whole-  
26 exome sequencing data from 18 different locations of a mCRC (Fig. 1A) under a powerful Bayesian  
27 framework, typical of organismal phylogenetics, phylodynamics and biogeography.

28  
29 After filtering out germline polymorphisms and single nucleotide variants (SNVs) in non-diploid  
30 regions, we detected 475 somatic SNVs with high confidence (Supplementary Table 1). A principal  
31 component analysis (PCA) of their allele frequencies showed a clear distinction between primary  
32 tumor and metastatic samples (Fig. 1B). Concordantly, we found a significant correlation  
33 between genetic and physical distances among these two groups, but not within (Supplementary  
34 Fig. 1). Albeit the extensive intratumor heterogeneity, we identified several clonal alterations in  
35 known CRC drivers<sup>11</sup>, including two copy neutral loss of heterozygosity events in *APC* and *TP53*,  
36 plus a non-synonymous mutation in *KRAS* (Fig. 1C-D). Moreover, we also observed a clonal non-  
37 synonymous mutation in *MSLN*, a plasma membrane differentiation antigen which is emerging  
38 as an attractive target for cancer immunotherapy due to its potential involvement in the  
39 epithelial-to-mesenchymal transition, a cellular process thought to be required for metastatic  
40 dissemination<sup>12</sup>.

41  
42 We obtained a Bayesian estimate of the phylogeny, under a relaxed clock model with exponential  
43 growth, of the 21 tumor clones identified (Fig. 2A). All the metastatic lineages grouped together  
44 with high support, suggesting a monoclonal origin. The age of the tumor was estimated to be  
45 6.94 – 6.45 years (95% Highest Posterior Density (HPD): 9.98/9.16 - 4.43/4.36) prior to clinical  
46 diagnosis (PCD). Also, the results imply an early origin of the metastatic ancestor, 4.20 years PCD  
47 (95% HPD: 6.30 - 2.46) (Supplementary Fig. 2), diverging within a short period of evolutionary  
48 time (posterior median divergence time = 2.58 years) from the ancestor of the tumor sample  
49 (tMRCA) (Fig. 2B). Despite the lack of a significant overall departure from neutrality across  
50 branches, evidence of positive selection (i.e., ratio of substitution rates at non-synonymous and  
51 synonymous sites ( $dN/dS$ ) > 1) was found for four specific branches in the phylogeny, including  
52 the ancestral lineage that gave rise to all the metastatic clones, pointing out to changes  
53 potentially relevant for the acquisition of metastatic capabilities (Fig. 2A). The most notable  
54 mutation in this branch was a non-synonymous mutation in *ANGPT4*, an angiogenic gene known  
55 to promote cancer progression in multiple cancer types<sup>13,14</sup>.

56  
57 Furthermore, the Bayesian skyline plot (Fig. 2C) shows that the tumor underwent a very rapid  
58 demographic expansion coincident with the diversification of both primary tumor and metastatic  
59 clades, before eventually becoming stationary. Interestingly, the expansion of the metastatic

60 clade seems to slightly precede the one associated with the primary tumor. The posterior median  
61 estimate of the population growth rate per generation was 0.014 (95% HPD: 0.006 - 0.03),  
62 implying an average population doubling time of 193 days.

63  
64 The colonization history of this tumor appears to have been quite complex. A dispersal-extinction  
65 biogeographic analysis placed the origin of sampled lineages around the geographical center of  
66 the primary tumor (Fig. 3A), subsequently radiating outwards in multiple directions. Additionally,  
67 we inferred with high confidence that the ancestral metastatic clone experienced an early long-  
68 distance dispersal to the liver (Fig. 3B), followed by a proliferation towards the nearby hepatic  
69 lymph nodes before eventually spreading “back” to the colonic lymph nodes. The number of  
70 implied migrations and movements was surprisingly high (Fig. 3C). Importantly, a distance-  
71 dependent model was heavily favored over a distance-independent model (Fig. 3D), suggesting  
72 an overall negative correlation between geographical distance and the dispersal ability of the  
73 tumoral clones at the whole patient level.

74  
75 Collectively, our analyses provide a detailed picture of the evolutionary history of this tumor.  
76 While we are not the first ones applying Bayesian phylogenetics for cancer dating<sup>8,9,15</sup>, previous  
77 attempts used sample trees and absence/presence mutational profiles instead of clonal  
78 phylogenies and clonal sequences, and therefore are subject to potential biases<sup>16,17</sup>. Besides, the  
79 evolutionary framework presented here has several advantages over previous approaches. For  
80 example, it is based on Bayesian estimates obtained only after contrasting competing  
81 evolutionary and demographic models under a rigorous model selection framework. Also, our  
82 biogeographic approach allows for the presence of the same ancestral clone at more than one  
83 location, and is able to consider the spatial distance among samples, unlike the approach of El-  
84 Kebir *et al.*<sup>17</sup>. On the other hand, our analyses imply a series of assumptions. In particular, it  
85 presumes that the clonal genotypes were appropriately reconstructed. Indeed, clonal  
86 deconvolution remains a very hard problem<sup>18</sup>, and we cannot rule out some degree of  
87 uncertainty in the precise combination of mutations assigned to any given clone. Nevertheless,  
88 we were reassured to some extent by the fact that comparable clonal genotypes were obtained  
89 when using a different deconvolution approach<sup>19</sup> (Supplementary Fig. 3). Moreover, our  
90 biogeographic model assumes that the geographical distances among samples more or less  
91 reflect the true “migration likelihood” of the tumoral clones. While we cannot prove that the  
92 distances used are realistic in this regard, different sets of distance matrices resulted in similar  
93 biogeographic solutions (Supplementary Fig. 4).

94  
95 Importantly, early metastases, such as the one described here, have already been proposed in  
96 mCRC<sup>8,9,15</sup>. Although Leung *et al.*<sup>20</sup> recently inferred a late-dissemination model in mCRC, they  
97 failed to provide quantitative measurements, and their timing of metastatic dissemination was

98 simply determined by visual inspection of mutational trees, making their results difficult to  
99 interpret and compare with. Reinforcing the idea of an early cell dissemination, our results  
100 suggest a fairly rapid population increase during the parallel phylogenetic diversification of the  
101 metastatic and primary tumor clades. Although these analyses revealed a similar individual  
102 contribution of each clade to the overall variation in effective population size, the observed  
103 demographic trends are compatible with an early geographical expansion, and subsequent  
104 establishment, of the metastatic lineages into new anatomical sites, together with the expansion  
105 of primary tumor populations to nearby areas.

106  
107 Our biogeographic reconstruction revealed a pattern of metastatic dissemination in which the  
108 primary tumor directly seeded liver metastases without an apparent early involvement of the  
109 lymphatic system. Previous studies have argued that metastatic spread in mCRC can potentially  
110 occur *via* the hepatic portal vein - a direct blood supply between the colon and the liver<sup>5,21</sup>. On  
111 this basis, metastatic dissemination in this patient seems to have started hematogenously, with  
112 a single episode of long-range dispersal across the hepatic portal vein into the liver, followed by  
113 a sequence of short-range migration episodes to nearby anatomical areas before eventually  
114 spreading to colonic lymph nodes. While the latter colonization has not yet been described in  
115 mCRC patients, it might represent some type of *self-seeding* mechanism, as previously observed  
116 in mCRC in mice<sup>22</sup>. Interestingly, we observed a similar migration pattern, albeit less detailed  
117 (Supplementary Fig. 5), using a different approach<sup>17</sup>.

118  
119 In conclusion, we believe that this study demonstrates the utility of a sound evolutionary  
120 framework for exploring the spatio-temporal dynamics of cancer cell populations from multi-  
121 regional sequencing data. By integrating concepts from population genetics, phylogenetics and  
122 biogeography, we were able to resolve the spatial architecture of this cancer, temporally connect  
123 phylogenetic events at time scales compatible with clinical observations, and recover past  
124 demographic changes shaping the spatial distribution of malignant clones. As more data  
125 continues to accumulate, future studies could extend these type of evolutionary analyses to  
126 other patients and cancer types, including polyclonal metastatic tumors<sup>5</sup>, in order to obtain a  
127 more comprehensive and meaningful understanding of the cancer spread, which could ultimately  
128 be used to predict clinical outcomes, and guide targeted treatments<sup>23</sup>.

129

## 130 **Methods**

131 **Sample collection.** A 51-year-old man was admitted to the University Hospital of Santiago de  
132 Compostela (CHUS) with a one-month history of weakness and weight loss. The patient died five  
133 days after admission, and the pathological assessment revealed a low-grade, moderately  
134 differentiated, adenocarcinoma of the descending colon, with multiple metastatic lymph-nodes,  
135 liver metastases, a metastatic focus in the right diaphragmatic peritoneum and multiple

136 intravascular micrometastases in both lungs (pT4aN2bM1c)<sup>24</sup>. During the warm autopsy,  
137 performed by JMC, a total of 18 samples were collected, including eight from the primary tumor  
138 (C1-C8), two from colonic lymph-node metastases (CL1, CL2), two from hepatic lymph-node  
139 metastases (HL1, HL2), four from liver metastases (L1-L4), and two healthy samples from the  
140 colon (N1, N2) (Fig. 1A). Sample collection was approved by a local ethics committee (CAEI Galicia  
141 2014/015), and written informed consent was provided by the patient's family.

142  
143 **Tumor disaggregation and sorting.** Tumor samples and normal CRC tissues were frozen in liquid  
144 nitrogen, placed in dry ice and transported to the laboratory. Next, samples were minced in  
145 pieces of 1 mm<sup>3</sup> with a scalpel and digested by incubation in Accutase (LINUS) for 1h at 37°C.  
146 Thereafter, the cell suspension was filtered with a 70 µm cell strainer (FALCON). The cell pellets  
147 were washed twice and suspended in ice-cold Phosphate Buffered Saline (PBS) and then stained  
148 for 30 min with the Anti-EpCAM (EBA1) antibody (BD). Following three successive washes in PBS  
149 buffer, flow cytometry analyses and sorting of EpCAM positive cells were performed with a  
150 FACSARIA III (BD Biosciences). Then, DRAQ5 and 7AAD dyes were added in order to select  
151 nucleated cells and exclude non-viable ones.

152  
153 **DNA extraction and exome sequencing.** The DNA was extracted from the 18 samples using the  
154 QIAamp DNA Mini kit (QIAGEN), and whole-exome sequencing was carried out at 60X with the  
155 Ion Torrent PGM platform at the Fundación Pública Galega de Medicina Xenómica (FPGMX) at  
156 Santiago de Compostela, Spain.

157  
158 **Detection of somatic variants.** Sequencing reads were aligned to the Genome Reference  
159 Consortium Human Build 37 (GRCh37) using the Torrent Mapping Alignment Program 5.0.7  
160 (TMAP). After alignment, single nucleotide variants (SNVs) were called independently for all  
161 tumor and normal samples using a standalone version of the Torrent Variant Caller 5.6.0 (TVC).  
162 Following a similar approach to de Leng *et al.*<sup>25</sup>, a set of high-stringency thresholds were used to  
163 retain high confidence bi-allelic calls, including a minimum coverage of 20X for both tumor and  
164 healthy samples, a minimum variant allele frequency (VAF) of 0.05, and a minimum nucleotide  
165 (Phred) quality score of 20. Germline polymorphisms were filtered by excluding variants present  
166 in the healthy samples. Copy number profiles, as well as tumor purity estimates and global ploidy  
167 status, were obtained using the Sequenza toolkit<sup>26</sup> under default settings (binning window of 1  
168 Mb).

169  
170 **Population structure.** To test the existence of population genetic structure in anatomical space,  
171 we assessed the correlation between genetic (measured *via*  $F_{ST}$  estimates) and geographical  
172 distance, using the Mantel test function in the adegenet R package<sup>27</sup> (Supplementary Fig. 1).

173

174 **Deconvolution of clonal populations.** Since the accuracy of the clonal deconvolution from mixed  
175 samples largely depends on the quality of the inferred VAFs, and copy-number variation is known  
176 to alter the allele frequency of somatic mutations in bulk tumor samples, somatic calls showing  
177 a VAF < 0.075, with a read depth < 20 in all tumor and healthy samples, and/or overlapping with  
178 copy-number events were filtered out prior to clonal deconvolution. The number of tumor  
179 clones, as well as their genotype sequences, were then inferred using the CloneFinder  
180 algorithm<sup>18</sup>, which has been previously shown to outperform other methods in both simulated  
181 and empirical datasets (but see Supplementary Information).

182  
183 **Bayesian phylogenetic model fitting, reconstruction and dating.** Bayesian phylogenetic analyses  
184 were performed using BEAST 2.4.7<sup>28</sup>. First, the most appropriate evolutionary model (i.e.,  
185 demographics and substitution rates) for our data was identified using Bayes factors<sup>29</sup>. A detailed  
186 description of the models tested can be found in Supplementary Table 2. For each candidate  
187 model, marginal likelihoods were obtained through a path-sampling analysis implemented in  
188 BEAST, using 100 independent Markov Chain Monte Carlo (MCMC) chains with 500,000 steps  
189 each. As a prior for the relaxed clock rate mean, a value of 4.6e-10 substitutions per site per  
190 generation derived experimentally for CRC<sup>15</sup> was used. For conversion to real time, a generation  
191 time of four days was assumed<sup>15,30</sup>. Moreover, since the clonal genotypes obtained only comprise  
192 variable genomic positions, an SNV ascertainment bias correction<sup>31</sup> was performed by modifying  
193 the “*constantSiteWeights*” attribute in the input XML file for BEAST. Posterior distributions under  
194 the model with highest support (i.e., Clock Model: Relaxed clock exponential; Tree: Coalescent  
195 Exponential Population) for the parameters of interest were obtained by running an MCMC chain  
196 during 100 million generations, sampled every 2000. Convergence was assessed using Tracer  
197 v1.6<sup>32</sup>. After discarding the first 10% of the samples as burn-in, point estimates for the different  
198 parameters were obtained using posterior means, and a maximum clade credibility topology was  
199 constructed using the median heights.

200  
201 **Demographic analysis.** Demographic changes in the cancer cell population were inferred from a  
202 Bayesian skyline plot (BSP) analysis carried out in BEAST 2.4.7. The same prior distributions  
203 described above were used, with the exception of the coalescent tree prior, which was set to  
204 “Coalescent Bayesian skyline”. The final skyline reconstruction was obtained using Tracer v1.6,  
205 setting the number of bins to 100 and the age of the youngest tip to 0 (i.e., the time of collection  
206 looking backwards).

207  
208 **Estimation of positive selection.** The coding clonal sequences were concatenated into a multiple  
209 sequence alignment and analyzed using PAML 4.8a<sup>33</sup> to obtain maximum likelihood estimates of  
210 the non-synonymous/synonymous rate ratio (*dN/dS*) for the different branches of the inferred  
211 clonal genealogy in BEAST. The significance of these estimates was tested using likelihood ratio

212 tests (LRTs) comparing a model assuming a single  $dN/dS$  for the whole genealogy (model M0) and  
213 models assuming that a specific branch has a different  $dN/dS$  than the rest (two-ratio model)<sup>34</sup>.

214

215 **Inference of ancestral clonal ranges and migration history.** The ancestral spatial distribution of  
216 the clones was reconstructed using BayArea<sup>6</sup> upon the inferred BEAST genealogy, together with  
217 the observed “geographic ranges” of the tumor clones (i.e., presence/absence of each clone at  
218 each of the 16 sampled locations of the tumor) (see Supplementary Information). Posterior  
219 distributions for the parameters of interest were obtained by running an MCMC chain during 100  
220 million steps, sampling every 2000 generations. BayArea implements a probabilistic dispersal-  
221 extinction biogeographic model that considers how different lineages colonize new regions or  
222 disappear from them through time. To examine whether two-dimensional geographical distances  
223 played a role in the dispersal ability of tumor clones, two candidate biogeographic models were  
224 compared in BayArea using Bayes factors (computed with the Savage-Dickey density ratio  
225 method): the mutual-independence (null) model, in which clonal dispersal is not conditioned by  
226 spatial distance (i.e., distance power parameter,  $\beta = 0$ ), versus a distance-dependent dispersal  
227 model, where the probability of dispersal is affected by spatial distance (i.e.,  $\beta > 0$ : dispersal to  
228 nearby areas is more likely than to distant locations, or  $\beta < 0$ : long-distance dispersal events are  
229 favored over short-distance movements). In order to define the spatial distances, different 2D  
230 coordinate matrices describing the geographical location of the samples were explored (see  
231 Supplementary Information).

## 232 References

- 233 1. Nowell, P. The clonal evolution of tumor cell populations. *Science* **194**, 23–28 (1976).
- 234 2. Gerlinger, M. *et al.* Intratumor heterogeneity and branched evolution revealed by multiregion  
235 sequencing. *N. Engl. J. Med.* **366**, 883–892 (2012).
- 236 3. Sottoriva, A. *et al.* A Big Bang model of human colorectal tumor growth. *Nat. Genet.* **47**, 209–216  
237 (2015).
- 238 4. Gerlinger, M. *et al.* Genomic architecture and evolution of clear cell renal cell carcinomas defined  
239 by multiregion sequencing. *Nat. Genet.* **46**, 225–233 (2014).
- 240 5. Naxerova, K. *et al.* Origins of lymphatic and distant metastases in human colorectal cancer. *Science*  
241 **357**, 55–60 (2017).
- 242 6. Landis, M. J., Matzke, N. J., Moore, B. R. & Huelsenbeck, J. P. Bayesian analysis of biogeography  
243 when the number of areas is large. *Syst. Biol.* **62**, 789–804 (2013).
- 244 7. Höhna, S. *et al.* RevBayes: Bayesian Phylogenetic Inference Using Graphical Models and an  
245 Interactive Model-Specification Language. *Systematic Biology* **65**, 726–736 (2016).
- 246 8. Lote, H. *et al.* Carbon dating cancer: defining the chronology of metastatic progression in colorectal  
247 cancer. *Ann. Oncol.* **28**, 1243–1249 (2017).
- 248 9. Zhao, Z.-M. *et al.* Early and multiple origins of metastatic lineages within primary tumors.  
249 *Proceedings of the National Academy of Sciences* **113**, 2140–2145 (2016).
- 250 10. Weinberg, R. A. Mechanisms of malignant progression. *Carcinogenesis* **29**, 1092–1095 (2008).
- 251 11. Vogelstein, B. & Kinzler, K. W. The Path to Cancer — Three Strikes and You’re Out. *New England*  
252 *Journal of Medicine* **373**, 1895–1898 (2015).
- 253 12. He, X. *et al.* Mesothelin promotes epithelial-to-mesenchymal transition and tumorigenicity of  
254 human lung cancer and mesothelioma cells. *Mol. Cancer* **16**, 63 (2017).
- 255 13. Brunckhorst, M. K., Xu, Y., Lu, R. & Yu, Q. Angiopoietins Promote Ovarian Cancer Progression by

- 256 Establishing a Procancer Microenvironment. *The American Journal of Pathology* **184**, 2285–2296  
257 (2014).
- 258 14. Lukas, R. V., Gondi, V., Kamson, D. O., Kumthekar, P. & Salgia, R. State-of-the-art considerations in  
259 small cell lung cancer brain metastases. *Oncotarget* **8**, 71223–71233 (2017).
- 260 15. Jones, S. *et al.* Comparative lesion sequencing provides insights into tumor evolution. *Proc. Natl.*  
261 *Acad. Sci. U. S. A.* **105**, 4283–4288 (2008).
- 262 16. Alves, J. M., Prieto, T. & Posada, D. Multiregional Tumor Trees Are Not Phylogenies. *Trends Cancer*  
263 *Res.* **3**, 546–550 (2017).
- 264 17. El-Kebir, M., Satas, G. & Raphael, B. J. Inferring parsimonious migration histories for metastatic  
265 cancers. *Nat. Genet.* **50**, 718–726 (2018).
- 266 18. Miura, S. *et al.* Predicting clone genotypes from tumor bulk sequencing of multiple samples.  
267 *Bioinformatics* (2018). doi:10.1093/bioinformatics/bty469
- 268 19. Popic, V. *et al.* Fast and scalable inference of multi-sample cancer lineages. *Genome Biol.* **16**, 91  
269 (2015).
- 270 20. Leung, M. L. *et al.* Single-cell DNA sequencing reveals a late-dissemination model in metastatic  
271 colorectal cancer. *Genome Res.* **27**, 1287–1299 (2017).
- 272 21. Mizuno, N., Kato, Y., Izumi, Y., Irimura, T. & Sugiyama, Y. Importance of hepatic first-pass removal in  
273 metastasis of colon carcinoma cells. *J. Hepatol.* **28**, 865–877 (1998).
- 274 22. Kim, M.-Y. *et al.* Tumor self-seeding by circulating cancer cells. *Cell* **139**, 1315–1326 (2009).
- 275 23. Tabassum, D. P. & Polyak, K. Tumorigenesis: it takes a village. *Nat. Rev. Cancer* **15**, 473–483 (2015).
- 276 24. Amin, M. B. *et al.* The Eighth Edition AJCC Cancer Staging Manual: Continuing to build a bridge from  
277 a population-based to a more ‘personalized’ approach to cancer staging. *CA: A Cancer Journal for*  
278 *Clinicians* **67**, 93–99 (2017).
- 279 25. de Leng, W. W. J. *et al.* Targeted Next Generation Sequencing as a Reliable Diagnostic Assay for the

- 280           Detection of Somatic Mutations in Tumours Using Minimal DNA Amounts from Formalin Fixed  
281           Paraffin Embedded Material. *PLoS One* **11**, e0149405 (2016).
- 282   26. Favero, F. *et al.* Sequenza: allele-specific copy number and mutation profiles from tumor  
283           sequencing data. *Ann. Oncol.* **26**, 64–70 (2015).
- 284   27. Jombart, T. adegenet: a R package for the multivariate analysis of genetic markers. *Bioinformatics*  
285           **24**, 1403–1405 (2008).
- 286   28. Bouckaert, R. *et al.* BEAST 2: a software platform for Bayesian evolutionary analysis. *PLoS Comput.*  
287           *Biol.* **10**, e1003537 (2014).
- 288   29. Kass, R. E. & Raftery, A. E. Bayes Factors. *Journal of the American Statistical Association* **90**, 773  
289           (1995).
- 290   30. Rew, D. A., Wilson, G. D., Taylor, I. & Weaver, P. C. Proliferation characteristics of human colorectal  
291           carcinomas measured in vivo. *Br. J. Surg.* **78**, 60–66 (1991).
- 292   31. Kuhner, M. K., Beerli, P., Yamato, J. & Felsenstein, J. Usefulness of single nucleotide polymorphism  
293           data for estimating population parameters. *Genetics* **156**, 439–447 (2000).
- 294   32. Rambaut, A., Drummond, A. J., Xie, D., Baele, G. & Suchard, M. A. Posterior Summarization in  
295           Bayesian Phylogenetics Using Tracer 1.7. *Systematic Biology* **67**, 901–904 (2018).
- 296   33. Yang, Z. PAML 4: Phylogenetic Analysis by Maximum Likelihood. *Molecular Biology and Evolution*  
297           **24**, 1586–1591 (2007).
- 298   34. Yang, Z. & Nielsen, R. Codon-substitution models for detecting molecular adaptation at individual  
299           sites along specific lineages. *Mol. Biol. Evol.* **19**, 908–917 (2002).

300

301 **Acknowledgements**

302 This work was supported by the European Research Council (ERC-617457- PHYLOCANCER  
303 awarded to D.P.) and by the Spanish Ministry of Economy and Competitiveness - MINECO  
304 (BFU2015-63774-P awarded to D.P.). D.P. receives further support from Xunta de Galicia. J.M.A.  
305 is currently supported by an AXA Research Fund Postdoctoral Fellowship. We want to thank Diana  
306 Valverde for her help with the DNA extractions from several samples. We want to additionally  
307 thank Nuria Estévez-Gómez, Pilar Alvariño and people from the Fundación Pública Galega de  
308 Medicina Xenómica (FPGMX) for their help with some of the experiments, and Tamara Prieto,  
309 Harald Detering, Diego Mallo, Laura Tomás and Sara Rocha for discussions. We also thank the  
310 Supercomputation Center of Galicia (CESGA) for providing computational resources.

311

312 **Author contributions**

313 D.P. conceived and supervised the study. J.M.C.T. obtained the tumor samples. S.P.L. processed  
314 the samples. J.M.A. performed all the analyses. J.M.A. and D.P. wrote the manuscript with input  
315 from all other authors.

316

317 **Competing interests**

318 The authors declare no competing interests.

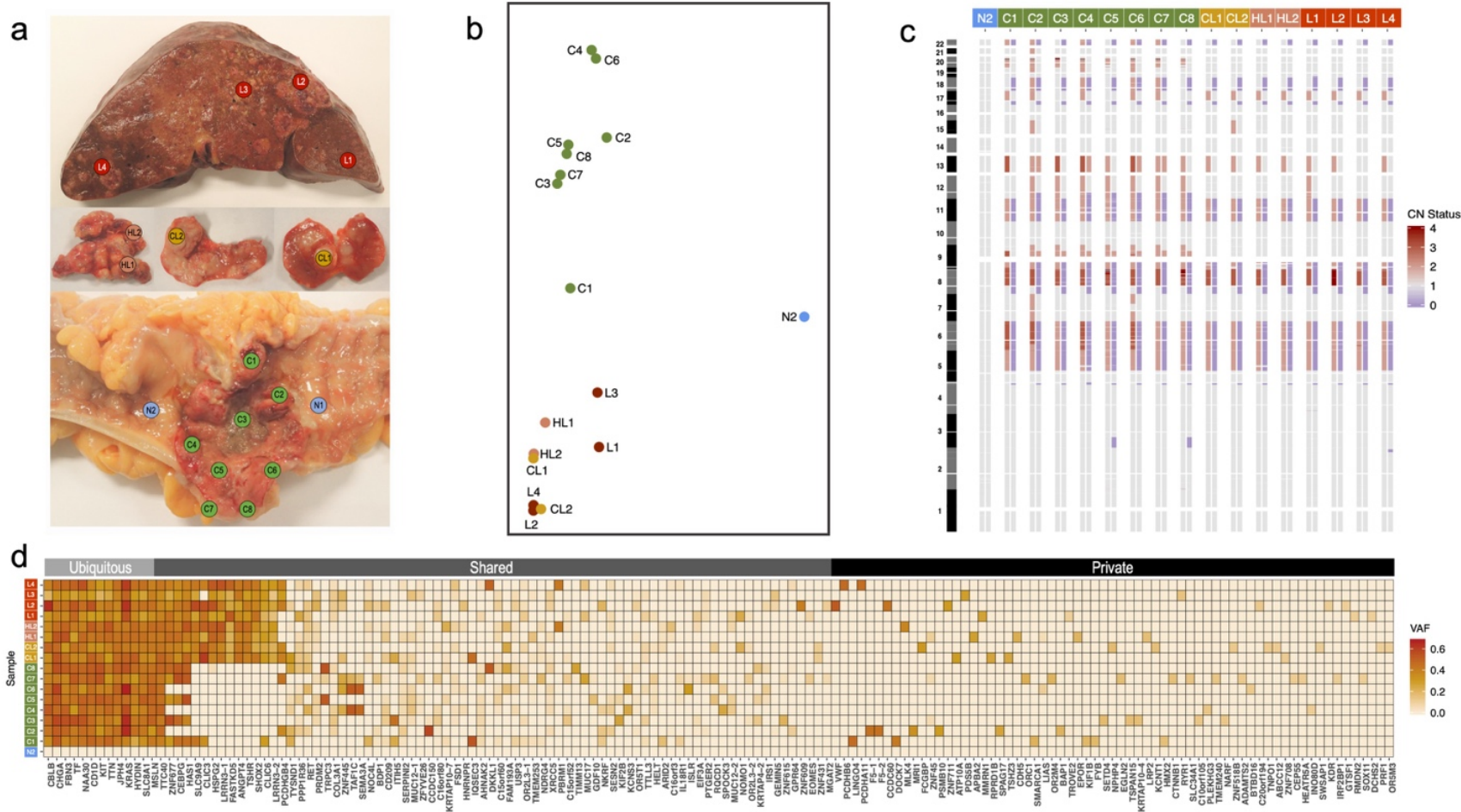


**Figure 1. Genomic profiles of bulk tumor samples.** **a**, Multiregional sampling scheme. A total of 18 samples were collected, including two samples from healthy tissue (in blue), eight from the primary tumor (green), two from proximal colonic lymph nodes (gold), two from distal hepatic lymph nodes (salmon), and four from liver metastasis (red). **b**, Principal component analysis (PCA) with variant allele frequencies (VAF) for all 475 somatic mutations detected. Each circle corresponds to a given sample, with colors highlighting the anatomical regions. **c**, Heatmap depicting genome-wide allele-specific copy number status (from 0 in blue to 4 in red) of healthy and tumor samples. Sample IDs are shown at the top. **d**, Heatmap with the observed allele frequencies (from 0 in white to 0.65 in red) of somatic mutations identified in the sequenced samples. Here only the non-synonymous mutations are shown ( $n = 156$ ), sorted according to their mean VAF across all tumor samples. Gene names are displayed at the bottom of the map. Each row represents a single sample.

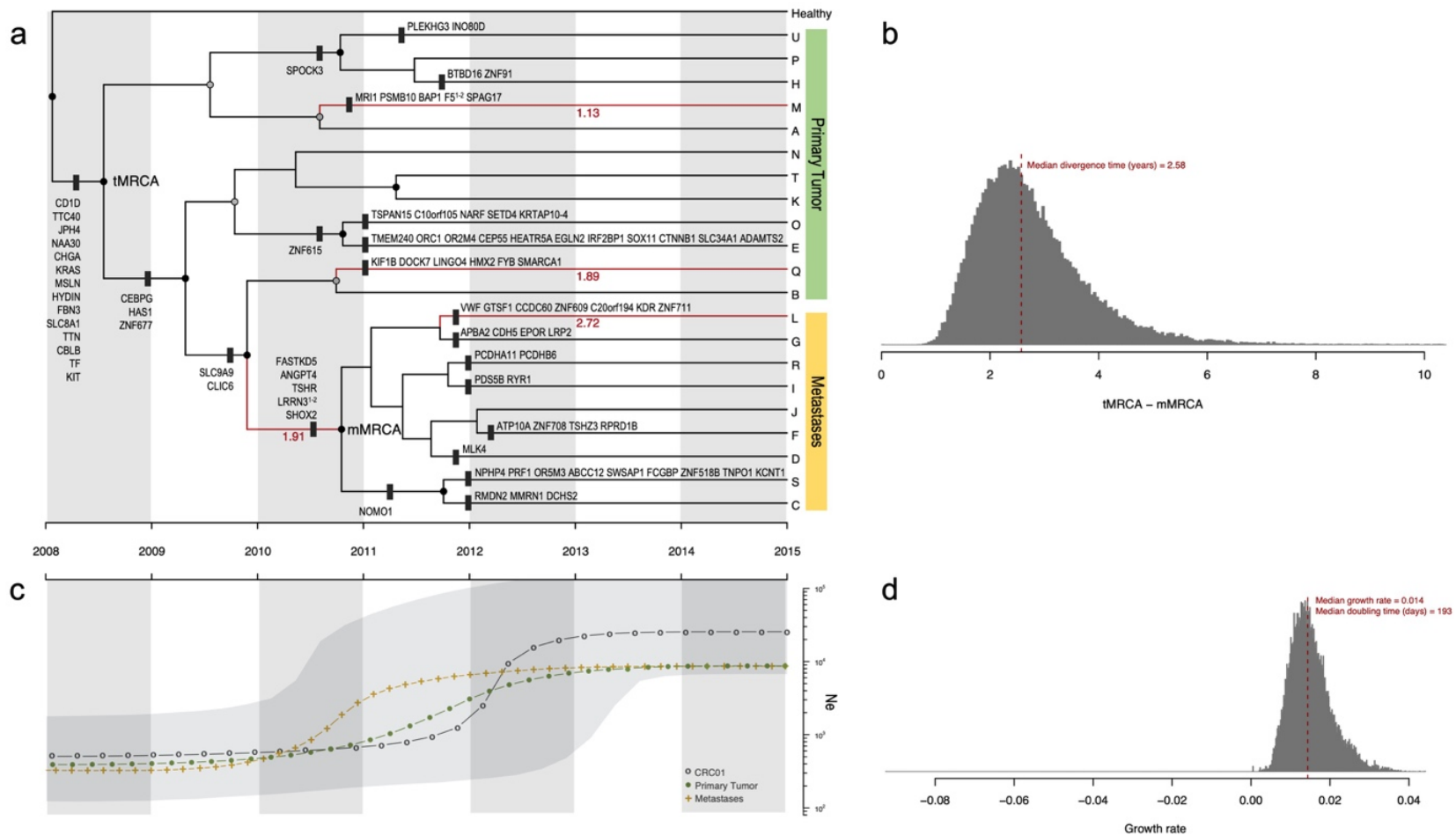


**Figure 2. Phylogenetic and demographic reconstruction over time.** **a**, Maximum clade credibility (MCC) tree resulting from the BEAST analyses using the CloneFinder-derived clones. Tree nodes with posterior probability values > 0.99 and > 0.50 are indicated with black and grey solid circles, respectively. Clone IDs (A-U) are shown at the tips of the tree. The x-axis is scaled to years (assuming one generation every four days; see Methods). Only non-synonymous mutations are shown. Tree branches showing a dN/dS ratio > 1 are highlighted in red together with the corresponding dN/dS value. **b**, Posterior probability distribution of the relative divergence time in years of mMRCA in relation to the tMRCA (tMRCA minus mMRCA). The dashed red line depicts the median age estimate of the mMRCA. **c**, Bayesian Skyline Plot (BSP) analysis. The y-axis is in log scale. The black dotted line represents the historical effective population size of the entire cancer cell population (Ne). The gray shading illustrates the 95% HPD interval. Green and golden dotted lines correspond to the effective population sizes of the primary and metastatic populations, respectively. **d**, Histogram illustrating the growth rate per generation of the tumor. The population doubling time is shown in days.

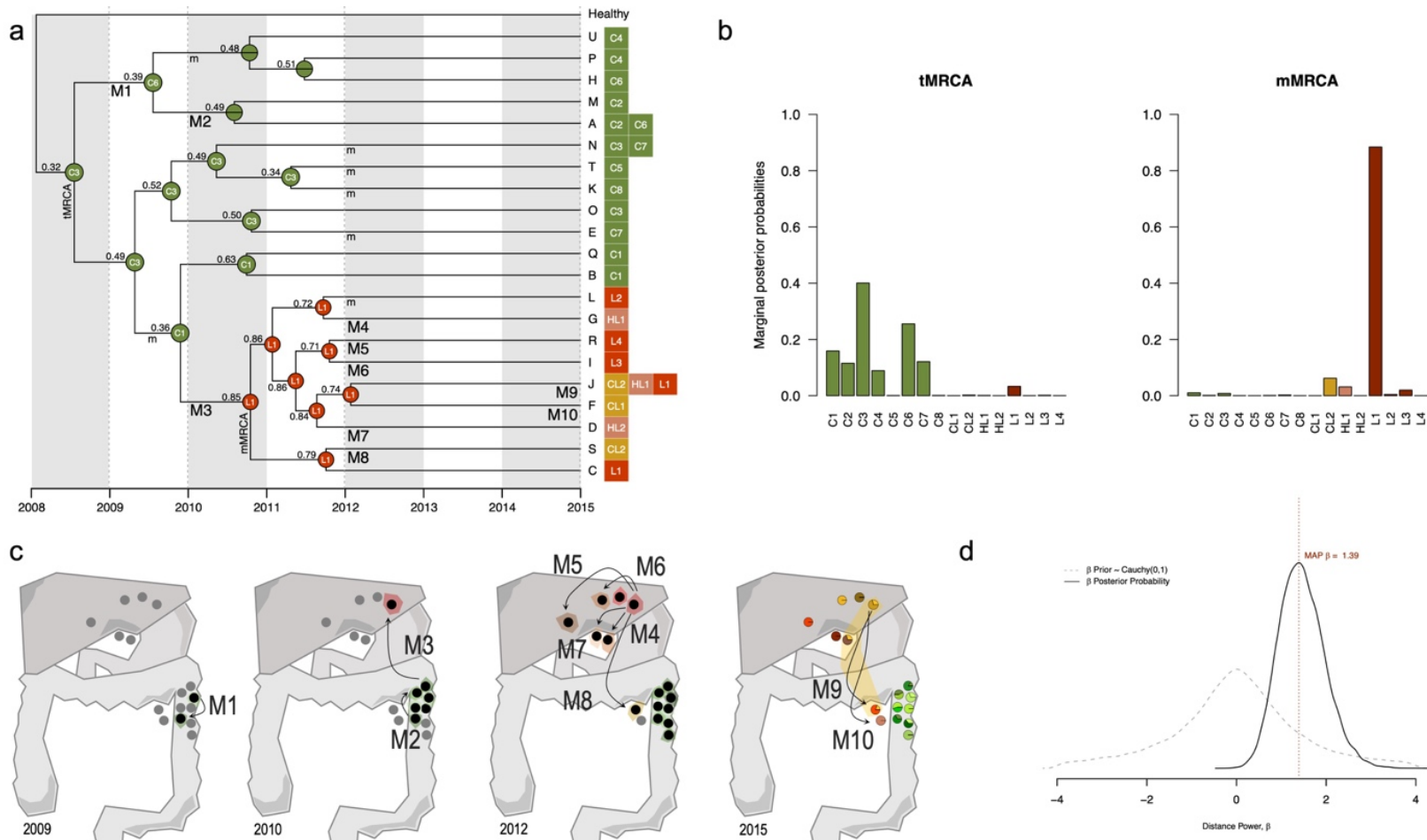


**Figure 3. Inferred biogeographic history.** **a**, Biogeographic reconstruction from BayArea, describing the geographical range (i.e., the set of occupied locations) of the ancestral clones. At each tree node, the range with the highest posterior probability is depicted. The sample ID is shown for those ancestral nodes whose inferred area ranges are restricted to a single location. The locations where the extant clones (A-U) were sampled are shown next to the tips. Migration events are depicted in the panel below represented by an uppercase “M” and numbered (M1-M10). A lowercase “m” indicates the remaining migrations inferred. **b**, Marginal posterior probabilities for the occupancy at single locations for the tumoral (tMRCA) and metastatic (mMRCA) ancestral clones. **c**, Schematic representation of the clonal dynamics in anatomical space over four time points. From 2009 to 2012, samples where BayArea inferred the presence of tumor clones are highlighted in black. Colored areas surrounding samples anatomical location represent the inferred spatial distribution of the clonal populations. Arrows highlight the inferred migration events. **d**, Comparison of the distance-dependent/independent dispersal models. The dashed grey line corresponds to the prior distribution for the distance power parameter,  $\beta \sim \text{Cauchy}(0,1)$ . The solid black line indicates the posterior distribution obtained. The vertical dashed red line indicates the maximum *a posteriori* estimate of  $\beta$ .